An Ins(1,4,5)P_3 receptor in *Paramecium* is associated with the osmoregulatory system

Eva-Maria Ladenburger*, Iris Korn, Nicole Kasielke, Thomas Wassmer and Helmut Plattner

Department of Biology, University of Konstanz, 78457 Konstanz, Germany

*Author for correspondence (e-mail: Eva.Ladenburger@uni-konstanz.de)

Accepted 1 June 2006
Journal of Cell Science 119, 3705-3717 Published by The Company of Biologists 2006
doi:10.1242/jcs.03075

Summary

In the ciliate *Paramecium*, a variety of well characterized processes are regulated by Ca^{2+}, e.g. exocytosis, endocytosis and ciliary beat. Therefore, among protozoa, *Paramecium* is considered a model organism for Ca^{2+} signaling, although the molecular identity of the channels responsible for the Ca^{2+} signals remains largely unknown. We have cloned – for the first time in a protozoan – the full sequence of the gene encoding a putative inositol (1,4,5)-trisphosphate (Ins(1,4,5)P_3) receptor from *Paramecium tetraurelia* cells showing molecular characteristics of higher eukaryotic cells. The homologously expressed Ins(1,4,5)P_3-binding domain binds [^{3}H]Ins(1,4,5)P_3, whereas antibodies unexpectedly localize this protein to the osmoregulatory system. The level of Ins(1,4,5)P_3-receptor expression was reduced, as shown on a transcriptional level and by immuno-staining, by decreasing the concentration of extracellular Ca^{2+} (*Paramecium* cells rapidly adjust their Ca^{2+} level to that in the outside medium). Fluorochromes reveal spontaneous fluctuations in cytosolic Ca^{2+} levels along the osmoregulatory system and these signals change upon activation of caged Ins(1,4,5)P_3. Considering the ongoing expulsion of substantial amounts of Ca^{2+} by the osmoregulatory system, we propose here that Ins(1,4,5)P_3 receptors serve a new function, i.e. a latent, graded reflux of Ca^{2+} to fine-tune $[Ca^{2+}]$ homeostasis.

Supplementary material available online at
http://jcs.biologists.org/cgi/content/full/119/17/3705/DC1

Key words: Ca^{2+}, Calcium, Inositol 1,4,5-trisphosphate, IP_3, Osmoregulation, *Paramecium*

Introduction

Increases in the concentration of intracellular Ca^{2+}, $[Ca^{2+}]_i$, govern a variety of processes in response to cell stimulation, such as exocytosis and cell contraction. A rise in intracellular Ca^{2+} may be due to Ca^{2+} influx from the outside medium or the activation of stores, such as the endoplasmic or sarcoplasmic reticulum (ER or SR). Stores may comprise Ca^{2+}-release channels of the inositol 1,4,5-trisphosphate [Ins(1,4,5)P_3] or ryanodine receptor (RyR) type (Berridge et al., 2000). Any latent, i.e. non-stimulated, activity of intracellular stores, and any involvement of such channels and their potential contribution to overall cell function, would be much less amenable to analysis than stimulated responses and, therefore, has so far not been described. We have now found evidence that such problems may occur in the osmoregulatory system (ORS) of *Paramecium*. We unexpectedly found that Ins(1,4,5)P_3 receptors (Ins(1,4,5)P_3R) are present in the ORS of *Paramecium* and that regulation of their expression depends on the Ca^{2+} concentration in the outside medium, $[Ca^{2+}]_o$.

Paramecium cells possess a vast system of cortical Ca^{2+}-storage compartments, the alveolar sacs (Stelly et al., 1991; Knoll et al., 1993), which are insensitive to Ins(1,4,5)P_3 (Laenge et al., 1995). The alveolar sacs contain Ca^{2+} in concentrations similar to those in skeletal muscle SR and are activated selectively during stimulated exocytosis of dense-core vesicles, which is induced by store-operated Ca^{2+} influx (reviewed in Plattner and Klauke, 2001). In the cell membrane, different types of Ca^{2+} channels have been characterized electrophysiologically (Machemer, 1988) and a Ca^{2+}-pump typical of the plasmalemma has been found (Wright and Van Houten, 1990). The vast ER system present throughout the cell has rather low levels of Ca^{2+} and contains a high-capacity, low-affinity Ca^{2+}-binding protein which differs from that in the alveolar sacs (Plattner and Klauke, 2001). An SR Ca^{2+} ATPase (SERCA)-type Ca^{2+}-ATPase is delivered from the ER to the alveolar sacs, where it is heavily enriched (Hauser et al., 1998; Kissmehl et al., 1998). Both the plasmalemmal as well as the SERCA-type Ca^{2+}-pump have low activity (Plattner and Klauke, 2001).

All this is in contrast to results from $^{45}Ca^{2+}$-flux studies in *Paramecium* cells, which revealed considerable basal influx rates without any stimulation (Browning and Nelson, 1976; Kerboeuf and Cohen, 1990; Knoll et al., 1992). In these reports, an important component for the regulation of homeostasis of intracellular Ca^{2+} concentration $[Ca^{2+}]_i$ in *Paramecium* cells was still undiscovered. For the following reasons, we assume that the ORS is involved in precisely such activities. Recently, the use of ion-selective electrodes revealed high Ca^{2+} levels in the fluid of the ORS (Stock et al., 2002a; Stock et al., 2002b). The ORS generally consists of two identical units per cell, each composed of a contractile vacuole, with approximately six collecting canals to which a tubular membranous network is attached (reviewed in Allen and Naitoh, 2002). This network displays a part proximal to the collecting canals that has smooth membranes (smooth spongiome) and a distal part that is studded with V-type H^+-

ATPase molecules (decorated spongiome). Since the vacuole fluid is expelled by rhythmic vacuole activity, this implies a major contribution of the ORS to $[Ca^{2+}]$ homeostasis in *Paramecium* cells. The system operates by a $[H^+]$ gradient, which is formed by the H^+-ATPase (Allen et al., 1990; Allen, 1995; Fok et al., 1995; Tominaga et al., 1998; Wassmer et al., 2005) and which might be coupled not only to the well-established osmotically driven water influx (Grønlien et al., 2002) but possibly also to a hypothetical cation-exchange system (Stock et al., 2002a; Stock et al., 2002b). In the absence of a Ca^{2+}-pump, Ca^{2+} might, thus, be transported into the ORS. Nevertheless, considering its excretory function, our current finding of Ca^{2+}-release channels in ORS membranes was rather surprising.

We here give the first thorough analysis of the gene encoding the Ins(1,4,5)P_3R in a protozoan. This was possible by having access to partial genomic sequences obtained by an international *Paramecium* genome project (Dessen et al., 2001; Sperling et al., 2002), based on an indexed genomic library (Keller and Cohen, 2000). The derived protein structure shows characteristics of an Ins(1,4,5)P_3R and we named the protein *Pt*IP_3R_N. Antibody (Ab) labeling shows specific localization of *Pt*IP_3R_N in the ORS and, moreover, when $[Ca^{2+}]_o$ is reduced, transcription of *Pt*IP_3R_N is downregulated. We propose a role of *Pt*IP_3R_N in the homeostasis of cytosolic $[Ca^{2+}]_i$ based on spontaneous $[Ca^{2+}]_i$ fluctuations seen along the ORS and the effect – although variable – uncaging Ins(1,4,5)P_3 has on these fluctuations. This putative function is new and might be considered the cellular equivalent of kidney function on a systemic level.

Results

Cloning of the gene encoding *Pt*IP_3R_N

A partial sequence resembling that of the Ins(1,4,5)P_3 receptor, M24E11u(rc), was isolated in a pilot genome project of *Paramecium* (Dessen et al., 2001; Sperling et al., 2002). In order to clone the gene, we screened an indexed genomic library (Keller and Cohen, 2000) in the laboratory of Jean Cohen (CNRS, Gif-sur-Yvette, France). By using probes designed from sequences of M24E11u(rc), four positive clones (28c10, 55d24, 113e9, 118e7) were identified and sequence analysis was extended to the original clone M24E11u(rc) by covering the 5′ region of the gene and reaching in the 3′ region up to bp 5171. A further extension of 1558 bp was done by primer walking using a genomic λZAPII library of *P. tetraurelia* (Hauser et al., 1998). Based on a current *Paramecium* genome project initiated by the Groupement de Recherches Européen (GDRE) and coordinated by Jean Cohen and Linda Sperling (CNRS, Gif-sur-Yvette, France) in collaboration with the Genoscope (Evry, France), sequences of the whole gene including flanking regions were obtained (Fig. 1A). cDNA sequences of the entire gene were amplified and cloned, revealing that the gene is expressed. Sequence analysis resulted in an open reading frame of 8670 bp coding for a protein of 2890 aa and a calculated molecular mass of 321 kDa. A comparison of the genomic sequence with their cDNA equivalent revealed six introns of 22 bp, 23 bp, 25 bp, 27 bp, 28 bp and 29 bp (Fig. 1A), a length typical for *Paramecium* (Russell et al., 1994; Sperling et al., 2002). The gene was named *IP_3R_N* (accession number CR932323).

Molecular structure of IP_3R_N

Ins(1,4,5)P_3 receptors are composed of an N-terminal ligand-binding domain, a central modulatory domain and a C-terminal channel domain with six membrane-spanning helices (reviewed in Bezprozvanny, 2005). The IP_3R_N protein possesses these size and topology characteristics. Deducing the amino acid sequence from IP_3R_N and performing a BLAST search using the NCBI database, the protein showed strongest similarity to the Ins(1,4,5)P_3 receptor type 3 (R3) from rat (Fig. 2) throughout its length, with an overall identity of 19% and similarity of 34% (Fig. 1B). Alignment and comparison of IP_3R_N with metazoan Ins(1,4,5)P_3 receptor sequences (Fig. 1E) show a relatively low degree of conservation of the *Paramecium* sequence in contrast to the close relationship of these proteins among metazoans.

The N-terminus of Ins(1,4,5)P_3 receptors [residues 224 to 579 of the mouse Ins(1,4,5)P_3R1] contains the crucial region for Ins(1,4,5)P_3 binding (Yoshikawa et al., 1996). Using the NCBI database, BLAST analysis of the corresponding region of the IP_3R_N gene product found 39% sequence identity and 49% similarity compared with rat Ins(1,4,5)P_3R3 (Fig. 1B). Of ten residues forming a basic pocket that interacts with the negatively charged phosphate groups of Ins(1,4,5)P_3 four are conserved in *Paramecium* (Fig. 2), including the three residues essential for specific binding in type 1 Ins(1,4,5)P_3 receptors (Yoshikawa et al., 1996). To get more evidence of whether this domain is able to bind Ins(1,4,5)P_3, we used the SWISS MODELL server for a 3D-alignment of the region with the published crystal structure of the mouse R1 Ins(1,4,5)P_3-binding domain (Bosanac et al., 2002). The model of the *Paramecium* Ins(1,4,5)P_3-binding domain (Fig. 1C) shows some differences from that of the mouse receptor structure but the central core appears quite similar.

Furthermore, a second domain, the RyR- and Ins(1,4,5)P_3R-homology (RIH) domain, was described that may provide a binding site for Ins(1,4,5)P_3 (Pointing, 2000). The RIH domain is found in the RyR and the Ins(1,4,5)P_3R and spans a region of 203 residues, starting in Ins(1,4,5)P_3R approximately at residue 1200. The conserved-domain database of the NCBI shows that this domain is also found in the Ins(1,4,5)P_3R sequence of *Paramecium* starting at residue 1331.

The channel domain of *Pt*IP_3R_N (residues 2447-2733) shares closest homology to type 3 RyRs. This is interesting, regarding the hypothesis that these channels represent a kind of hybrid between RyRs and Ins(1,4,5)P_3 Rs, as postulated for intracellular Ca^{2+}-release channels in the related unicellular parasite *Toxoplasma gondii* (Lovett et al., 2002). We found that the close relationship of the channel domain in IP_3R_N and RyRs might be due to a loop between transmembrane region 5 and the pore region present in the rat Ins(1,4,5)P_3R3 (residues V2398-A2453), which is missing in the *Paramecium* sequence as well as in RyRs. Moreover, analysis of the deduced amino acid sequence and hydrophobicity analysis (Fig. 1D) shows that the C-terminus of IP_3R_N contains six membrane-spanning helices that have the pore region lying between transmembrane domain 5 and 6, which is characteristic of all Ins(1,4,5)P_3 channels. There is also a high degree of sequence identity (up to 50%) in the transmembrane regions 5 and 6 and in the pore-forming region (Fig. 2).

On the basis of the overall size and topology, we propose that the IP_3R_N is related to intracellular Ca^{2+}-channels of the

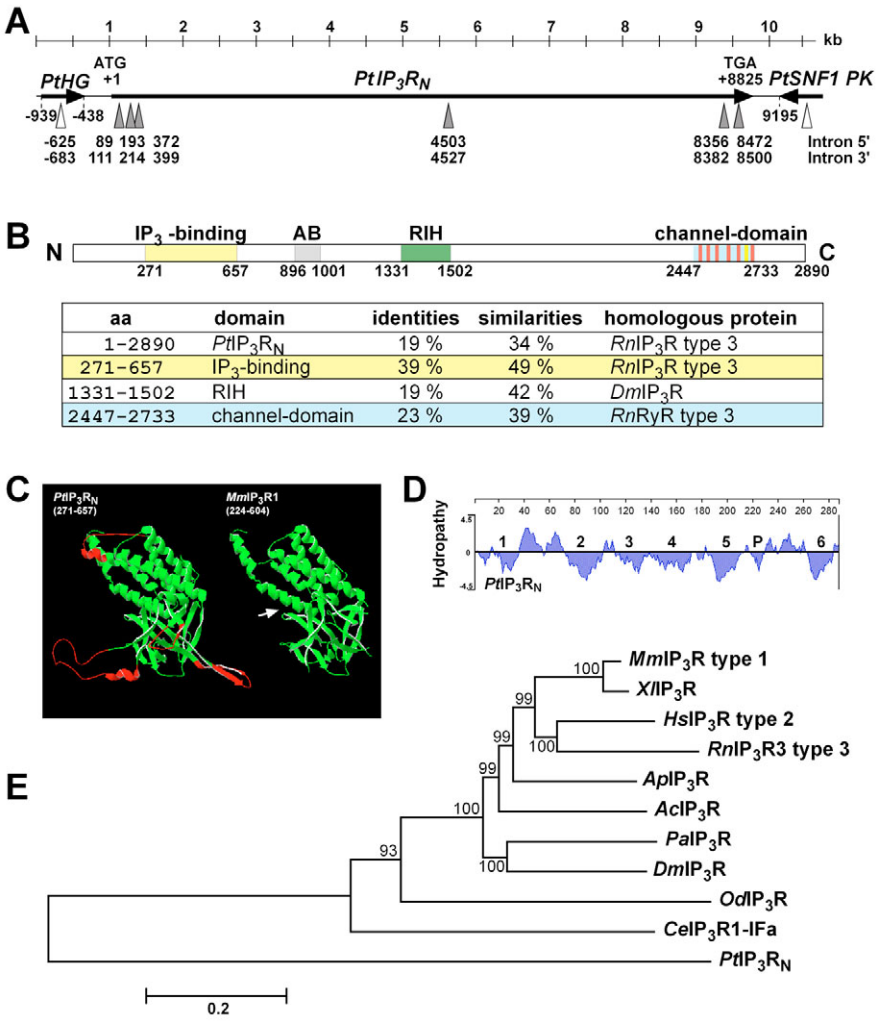

aa	domain	identities	similarities	homologous protein
1-2890	*Pt*IP$_3$R$_N$	19 %	34 %	*Rn*IP$_3$R type 3
271-657	IP$_3$-binding	39 %	49 %	*Rn*IP$_3$R type 3
1331-1502	RIH	19 %	42 %	*Dm*IP$_3$R
2447-2733	channel-domain	23 %	39 %	*Rn*RyR type 3

Fig. 1. Molecular characterization of *Pt*IP$_3$R$_N$. (A) Schematic representation of macronuclear sequences of the *PtIP$_3$R$_N$* gene from *P. tetraurelia* (*Pt*): The *PtIP$_3$R$_N$* gene is flanked upstream by a gene (*PtHG*) homologous to hemoglobin of *Paramecium triaurelia* (Yamauchi et al., 1995), accession number S60032, and downstream by a gene (*PtSNF1 PK*) homologous to a putative SNF1-related protein kinase [(Zagulski et al., 2004), accession No YP_054292]. Start (+1) and stop codons (+8825) of IP$_3$R$_N$ were determined by RT-PCR, likewise introns, which are shown as triangles. The positions of the introns are indicated at nucleotide level at 5′ (intron 5′) and 3′ end (intron 3′). (B) Domain structure of the *Paramecium* Ins(1,4,5)P_3 receptor IP$_3$R$_N$. Results of sequence analysis of single domains are summarized in the table. (C) Modeling of the Ins(1,4,5)P_3-binding domain using the Swiss-Model homology-modeling server (Peitsch and Jongeneel, 1993). (Right) Published structure of the Ins(1,4,5)P_3-binding region of mouse Ins(1,4,5)P_3 receptor type 1 (Bosanac et al., 2002); (left) model of the *Paramecium* Ins(1,4,5)P_3-binding region. Areas that were aligned are shown in green, red regions are not compatible to the given structure. The arrow indicates the Ins(1,4,5)P_3-binding site. (D) Hydrophobicity analysis of the channel domain of IP$_3$R$_N$ reveals six transmembrane regions. (E) Evolutionary relationship of the *Paramecium* IP$_3$R$_N$ protein. Predictions from multiple sequence alignments are shown in a neighbor-joining tree with 1000 bootstrap replicates generated with the MEGA version 3.0 program. Sequences representing the three different types of mammalian Ins(1,4,5)P_3 receptors were from *Mus musculus* (*Mm*IP$_3$R type 1, P11881), *Homo sapiens* (*Hs*IP$_3$R type 2, Q14571) and *Rattus norvergicus* (*Rn*IP$_3$R type 3, AAA41446). Other metazoan IP$_3$R sequences were from *Aplysia californica* (*Ac*IP$_3$R, ABD62080), *Oikopleura dioica* (*Oc*IP$_3$R, AAT47836), *Caenorhabditis elegans* (*Ce*IP$_3$R1-IFa, AAW30668), *Xenopus laevis* (*Xl*IP$_3$R, BAA03304), *Drosophila melanogaster* (*Dm*IP$_3$R, BAA14399), *Panulirus argus* (*Pa*IP$_3$R, AAC61691) and *Asterina pectinifera* (*Ap*IP$_3$R, BAB84088). Bootstrap support values are given above the branches and evolutionary distances are indicated by the scale bar below.

Ins(1,4,5)P_3 receptors, notably the type 3 receptor of mammals.

Determination of Ins(1,4,5)P_3 binding to the putative Ins(1,4,5)P_3-binding domain of IP$_3$R$_N$

Because the putative Ins(1,4,5)P_3-binding domain of IP$_3$R$_N$ is less conserved than in other Ins(1,4,5)P_3 receptors of metazoans, we examined Ins(1,4,5)P_3 binding to this domain. To avoid mutating all deviant 23 *Paramecium* glutamine codons to universal glutamine codons, this region was expressed directly in *Paramecium*. Therefore, we constructed a GFP-fusion protein, in which GFP was fused to the C-terminus of residues T267-L657 of IP$_3$R$_N$, using the pPXV-GFP vector. The fusion construct or the GFP-vector alone (control) were microinjected into the macronucleus of *Paramecium* cells and overexpression was monitored by GFP-fluorescence (Fig. 3A). As expected, overexpression of GFP alone leads to a fluorescent signal throughout the cell, including the macronucleus; overexpression of GFP-IP$_3$BD leads to a fluorescent signal only in the cytosol, in agreement with the calculated mass (~72 kDa) of GFP-IP$_3$BD. Transformed cell clones were propagated and purification of GFP and GFP-IP$_3$BD proteins was performed by immuno-precipitation using Abs against GFP. To confirm a successful precipitation, one-third of precipitated proteins were analyzed by immuno-blotting (Fig. 3B). As shown in Fig. 4B, GFP-specific Abs efficiently precipitated the recombinant proteins GFP and GFP-IP$_3$BD (Fig. 3B, lanes 2 and 4), whereas control IgGs did not (Fig. 3B, lanes 1 and 3).

By using GFP- or GFP-IP$_3$BD-coupled protein-A agarose beads, [^{3}H]Ins(1,4,5)P_3 binding experiments were carried out (Fig. 3C). We found a two- to threefold enrichment of [^{3}H]Ins(1,4,5)P_3 bound to GFP-IP$_3$BD beads compared with GFP-coupled beads. The binding specificity of GFP-IP$_3$BD beads has been shown by competition with 10 μM non-radiolabeled Ins(1,4,5)P_3, which reduced [^{3}H]Ins(1,4,5)P_3 binding close to background level (Fig. 3C right panel).

Immunofluorescence localization and western blots

To analyze the subcellular distribution of IP$_3$R$_N$, we raised a polyclonal antiserum to a recombinant polypeptide corresponding to IP$_3$R$_N$ residues R896-Q1001 (Fig. 2). As shown in Fig. 4A, affinity-purified anti-

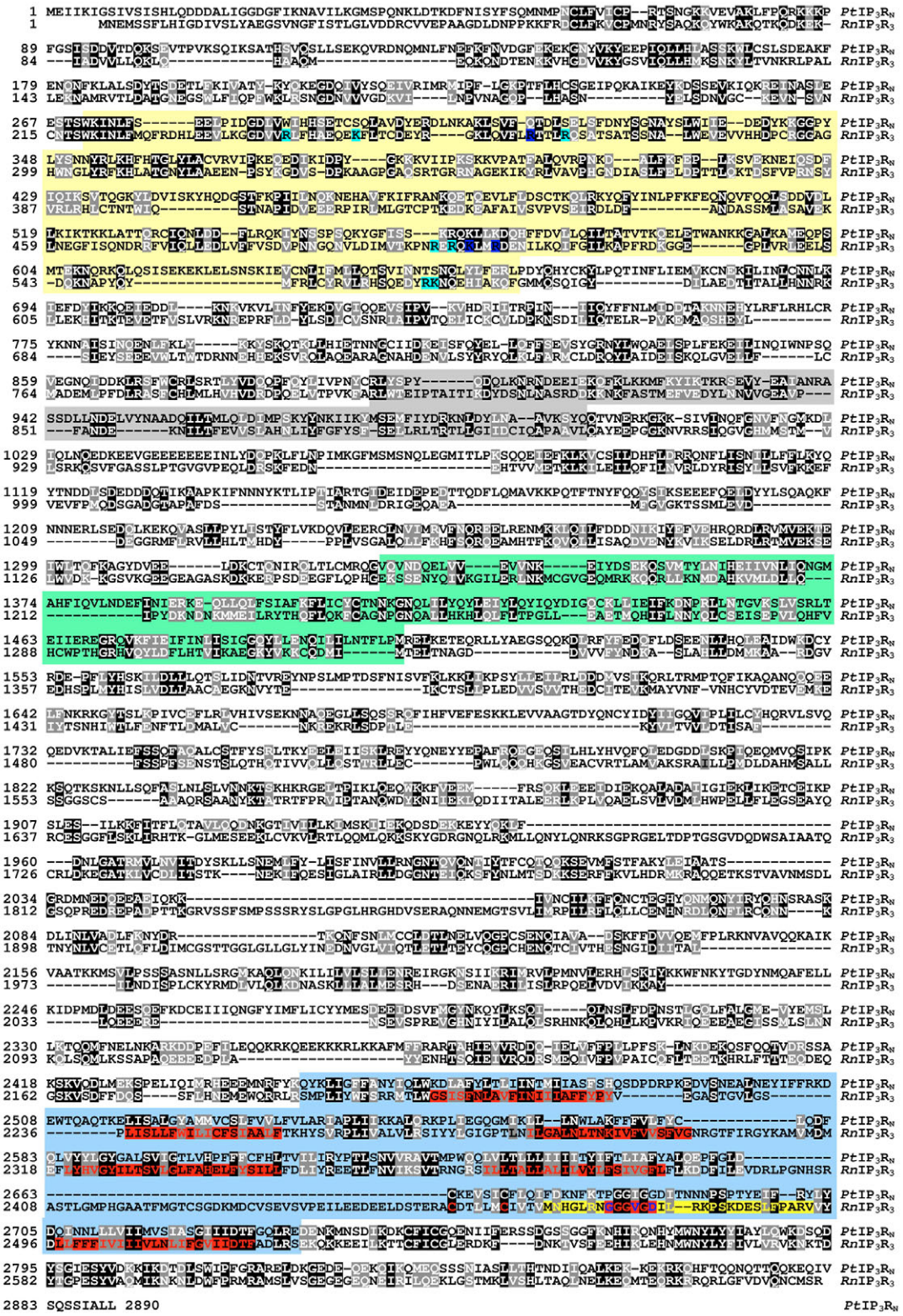

Fig. 2. Sequence analysis of IP_3R_N. Alignment of *Pt*IP_3R_N and rat Ins(1,4,5)P_3R3 (*Rn*IP_3R3) using the 'Blast 2 Sequences' tool (Tatusova and Madden, 1999). Sequences are shown in single-letter code and are numbered on the left side. Residues that are identical are shaded black, similar residues are shaded gray. The putative binding region for Ins(1,4,5)P_3 is boxed in yellow. Amino acids shaded blue are involved in Ins(1,4,5)P_3-binding, those bordered in dark blue are essential for Ins(1,4,5)P_3-binding (Yoshikawa et al., 1996). The homology domain for Ins(1,4,5)P_3Rs and RyRs (RIH-domain) is boxed in green, the channel domain in light blue. The six transmembrane regions are highlighted in red, the pore region in yellow. The antigenic region used to raise a polyclonal Ab is boxed in gray. Rat Ins(1,4,5)P_3R3 sequences (accession number L06096) are published by Blondel et al. (Blondel et al., 1993).

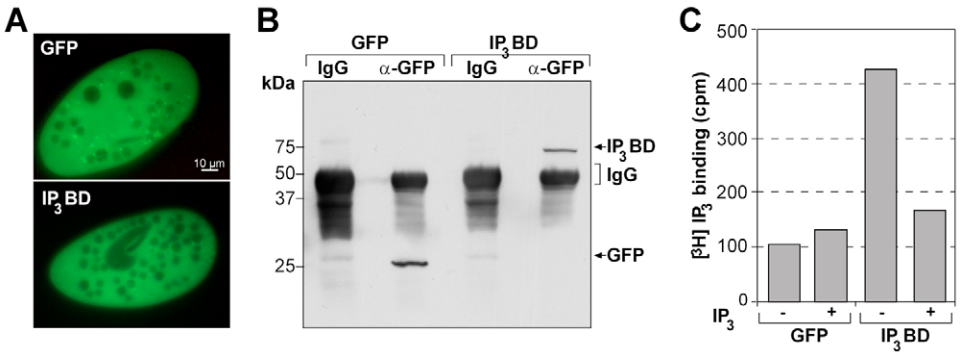

Fig. 3. Expression and [^{3}H]Ins(1,4,5)P_3-binding activity of the putative Ins(1,4,5)P_3-binding domain of *Pt*IP$_3$R$_N$. (A) Overexpression of GFP alone (top) and GFP fused to the putative Ins(1,4,5)P_3-binding domain (IP$_3$BD) of IP$_3$R$_N$ (bottom) in *Paramecium* 7S cells. (B) Western blot analysis of immuno-precipitated GFP-IP$_3$BD fusion protein or GFP alone with GFP-specific Ab. (C) [^{3}H]Ins(1,4,5)P_3- ([^{3}H] IP$_3$) binding assay using agarose beads coupled to protein A either with GFP alone or with GFP-IP$_3$BD fusion protein. Inhibition of specific [^{3}H]Ins(1,4,5)P_3-binding was measured in the presence of 10 μM cold Ins(1,4,5)P_3. The graph represents one out of five experiments.

IP$_3$R$_N$ Abs recognize the polypeptide with high affinity in western blots. To ensure a specific interaction with IP$_3$R$_N$, the same Abs were used to investigate insoluble fractions (100,000-***g*** pellet) of whole-cell homogenates. In immuno-blots anti-IP$_3$R$_N$-Abs recognize a high-molecular-mass band of ~250 kDa (Fig. 4B). An additional band of 37 kDa is probably a degradation product of IP$_3$R$_N$, because the ratio of the two bands changes depending on the protease inhibitor concentration applied during preparation (data not shown). The detected proteins were completely extracted when 100,000-***g*** pellets were treated with 1.5% (data not shown) or 2% Triton X-100 (Fig. 4B) as usual for membrane proteins like Ins(1,4,5)P_3Rs (Serysheva et al., 2003).

The intracellular localization of IP$_3$R$_N$ was determined by immunofluorescence analysis of permeabilized cells by using a polyclonal Ab specific for IP$_3$R$_N$. As shown in Fig. 4C, Abs bind to the ORS, resulting in regular labeling around the radial arms, the central vacuole and the ampullae connecting both these structures. This staining pattern is independent of the fixation or permeabilization protocol applied (0.5% digitonin or 1% Triton X-100).

Immuno-gold electron microscopy (EM) analyses showed presence of IP$_3$R$_N$ at the smooth spongiome and possibly along the collecting canals but its absence from the decorated spongiome. The labeling density was >20:1. Considering its vast extension of membrane tubules, the smooth spongiome may harbor most of the IP$_3$R$_N$-type Ca^{2+}-release channels (Fig. 5).

Effects of lowering $[Ca^{2+}]_o$

In addition to water regulation, various observations suggest that, in *Paramecium* cells, the ORS extrudes Ca^{2+} (Stock et al., 2002a; Stock et al., 2002b). We therefore investigated whether there is a correlation between $[Ca^{2+}]_o$ and *IP$_3$R$_N$* gene expression. By raising $[Ca^{2+}]_o$ from 1 mM to 10 mM no change in IP$_3$R$_N$ expression was observed (data not shown). By contrast, gene expression of IP$_3$R$_N$ is reduced when cells are exposed to low $[Ca^{2+}]_o$. Immunofluorescence analyses showed that the labeling of the ORS with IP$_3$R$_N$-specific Abs at different stages is reduced, whereas the staining pattern obtained with Abs against the V-type H^+-ATPase (Wassmer et al., 2006) is not influenced (Fig. 6A) under these conditions. Similar results could be obtained by analyzing RNA levels by RT-PCR, using primers against an actin isoform (actin8-1) as control. As shown in Fig. 6B and C, the amount of amplified samples of the actin isoform does not change, whereas a decrease of product expression was observed when IP$_3$R$_N$-specific primers were used.

Since an $[Ca^{2+}]_o$ at 1 μM is the limiting concentration for our cells to survive, we examined whether the ORS activity is affected when cells were incubated at varying $[Ca^{2+}]_o$. However, this does not effect the pumping activity of the ORS, because no significant differences in contraction periods were observed under the varying conditions and their maximal diameter of ~9 μm remained unaffected (data not shown).

Effects of exposure to LiCl

Li^+ interferes with the phospho-inositol cycle by inhibiting phospho-inositol-monophosphatases (Hallcher et al., 1980; Gee et al., 1988), leading to reduced formation of Ins(1,4,5)P_3. Since several reports had indicated that *Paramecium* possesses targets for LiCl (Beisson and Ruiz, 1992; Wright et al., 1992), we examined whether Li^+ has an effect on IP$_3$R$_N$.

LiCl (25 mM) was added to growing populations of *P. tetraurelia* for 2, 3 and 4 hours, followed by immunofluorescence analysis. We found significant changes in the labeling of cells stained with IP$_3$R$_N$-specific Abs; and the extent of these changes depended on $[Ca^{2+}]$ in the culture media, which normally is 100 μM. By lowering $[Ca^{2+}]_o$ to 1 μM we could amplify the Li^+ effect to a maximum after 3 hours of Li^+ treatment (Fig. 7A). Although Ab labeling is decreased and/or redistributed to a speckled pattern in aliquots incubated with Li^+ (Fig. 7A; left panel), control cells incubated with Na^+ show the same staining as untreated cells. After exposure to Li^+, we could not detect any changes in *IP$_3$R$_N$* mRNA levels (data not shown). Therefore, we assume that (in contrast to the observations with varying $[Ca^{2+}]_o$, Li^+ mainly causes IP$_3$R$_N$ redistribution rather than affecting the levels of IP$_3$R$_N$. The effect of Li^+ is restricted specifically to IP$_3$R$_N$ because the staining pattern of the ORS with Abs against V-type H^+-ATPase does not change (Fig. 7A; right panel). Furthermore, these experiments indicate that the decorated spongiome remains attached to the organelle.

Li^+ also clearly affected the activity of contractile vacuoles independently of $[Ca^{2+}]_o$. Incubation of *P. tetraurelia* in 25 mM

LiCl for 3 hours decreased vacuolar activity significantly (Fig. 7B). When cells were allowed to recover for 3 hours in culture medium without Li^+, contraction periods returned to normal values, indicating that the Li^+ effect was reversible. Although the Li^+ effect was not investigated in more detail, our data suggest that ORS activity is under latent control of IP_3R_N activity.

Ca^{2+} imaging studies

A functional Ins(1,4,5)P_3R is usually determined by significant Ca^{2+} release in response to formation of Ins(1,4,5)P_3 after stimulation. To visualize Ca^{2+} release, we used high-affinity dextran-coupled Fluo-4, a derivative that, due to its size, stays in the cytosol. This was either used to monitor spontaneous $[Ca^{2+}]_i$ oscillations near the ORS or combined in injections with NPE-caged Ins(1,4,5)P_3. The ability of our microscopical set-up to activate caged compounds by UV-light was tested with DMNB-caged fluorescein-coupled dextran (10,000 kDa), which can be uncaged efficiently (data not shown). Thus dextran-coupled Fluo-4 was injected with or without NPE-caged Ins(1,4,5)P_3. As soon as the fluorochrome was evenly distributed in the cell, we started recording (Figs 8-10) in different locations of the cell, including regions of the ORS containing the spongiome, where IP_3R_N was localized by immuno-EM (Fig. 5).

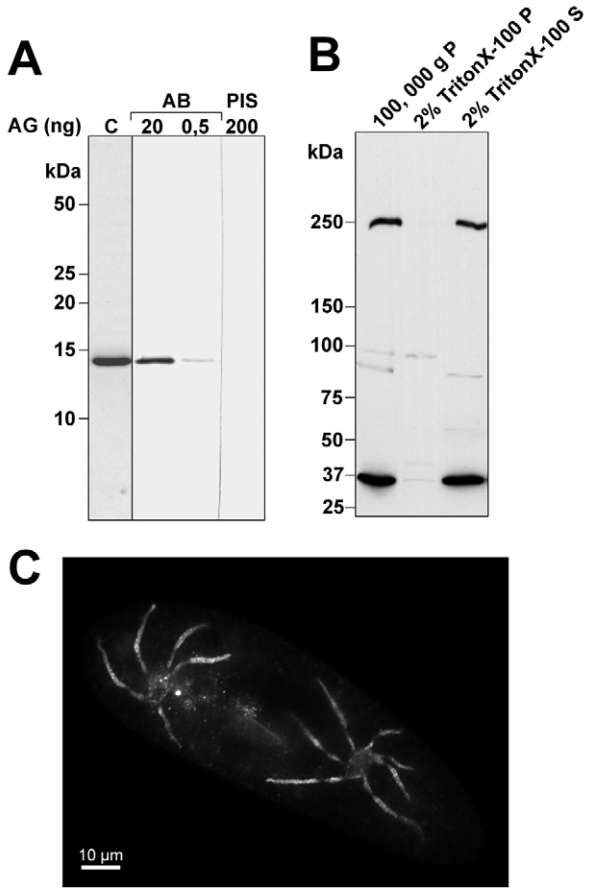

Fig. 4. Characterization of polyclonal antibodies against IP_3R_N. (A) Affinity-purified anti-IP_3R_N Abs recognize the polypeptide corresponding to IP_3R_N residues R896-Q1001 (AG) with high affinity in immuno-blots (second and third lanes), whereas the preimmunserum (PIS) does not show any interaction (fourth lane). The first lane, C, shows 2 μg of the purified AG (Coomassie Blue-stained) used for immunization. (B) Western blot analysis using anti-IP_3R_N Abs. 100,000-***g*** pellet of whole *Paramecium* cell homogenate (left lane) was extracted with 2% Triton X-100 and insoluble proteins (middle lane) were separated from soluble proteins (right lane). (C) Subcellular distribution of IP_3R_N in *Paramecium* cells. Immunofluorescence analysis shows that Abs against IP_3R_N stain the ORS.

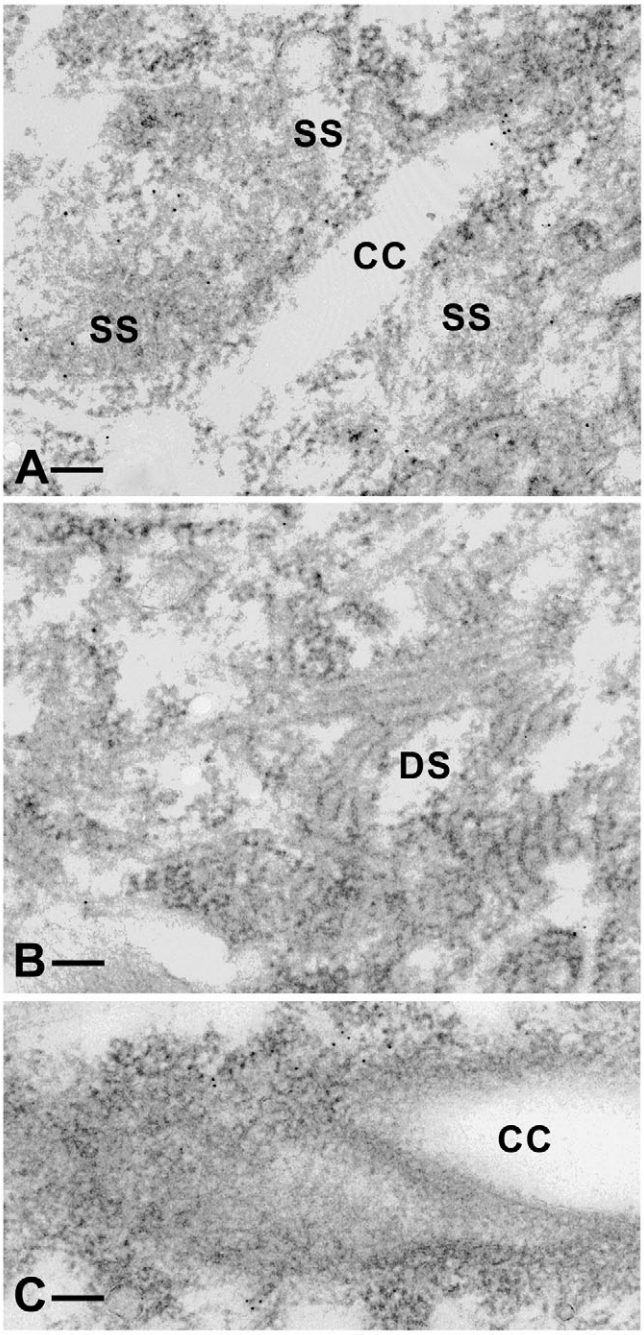

Fig. 5. Immuno-gold EM localization of *Pt*IP_3R_N. (A,B) Dense labeling (gold grains) occurs in the layer around the collecting canals (CC) and represents the smooth spongiome (SS) (A), whereas the decorated spongiome (DS) shows only few gold grains (B). (C) Labeling also occurs directly adjacent to the lumen of the collecting canal. Bars, 0.1 μm.

First, spontaneous Ca^{2+} sparks were seen along parts of the ORS when Ins(1,4,5)P_3 was not uncaged (Fig. 8). These signals were superimposed by Ca^{2+} oscillations, one such wave is shown in Fig. 8. Such spontaneous Ca^{2+} oscillations, with periods of approximately 8-20 seconds, were frequently observed in baseline recordings before uncaging with UV (Figs 9, 10). The maximum of these Ca^{2+} signals was detected anywhere between the systolic phase of the contractile vacuole and the diastolic phase, thus the recorded fluorescence differences cannot be simply due to a change in volume. Also, periods of ORS contraction activity and Ca^{2+} signals were not strictly identical.

In addition to the Ca^{2+} oscillations, we found spontaneous Ca^{2+} signals traveling along the radial arms of the ORS (Fig. 8A, supplementary material Movies 1 and 2). This observation was confirmed by the ratio of evaluated line tracings of distinct cellular regions (Fig. 8B). Traces obtained from spots in close proximity to the ampullae (traces b, c) or the radial arms (trace a) show additional Ca^{2+} peaks compared with trace d, obtained from a region more distant to the ORS. Trace d represents the large Ca^{2+} signal of an oscillation wave, enhancing the small additional Ca^{2+} sparks visualized in traces a to c. This finding agrees with a localization of IP_3R_N to the smooth spongiome (Fig. 5). Enhancement of the small, locally confined Ca^{2+} signals (Fig. 8) may result in larger, eventually oscillating signals. This supports the regulation of localised $[Ca^{2+}]_i$ via the ORS, by sequestration and partial reflux.

To test the involvement of Ins(1,4,5)P_3 in these Ca^{2+}-dynamics, we raised the concentration of intracellular Ins(1,4,5)P_3 by uncaging Ins(1,4,5)P_3 in the cytosol. In Figs 9 and 10, respectively, we present Ca^{2+} oscillations before and after the release of Ins(1,4,5)P_3, followed by evaluation of different cell regions. In both cases, a change in Ca^{2+} oscillations after UV treatment is seen. Results are similar at

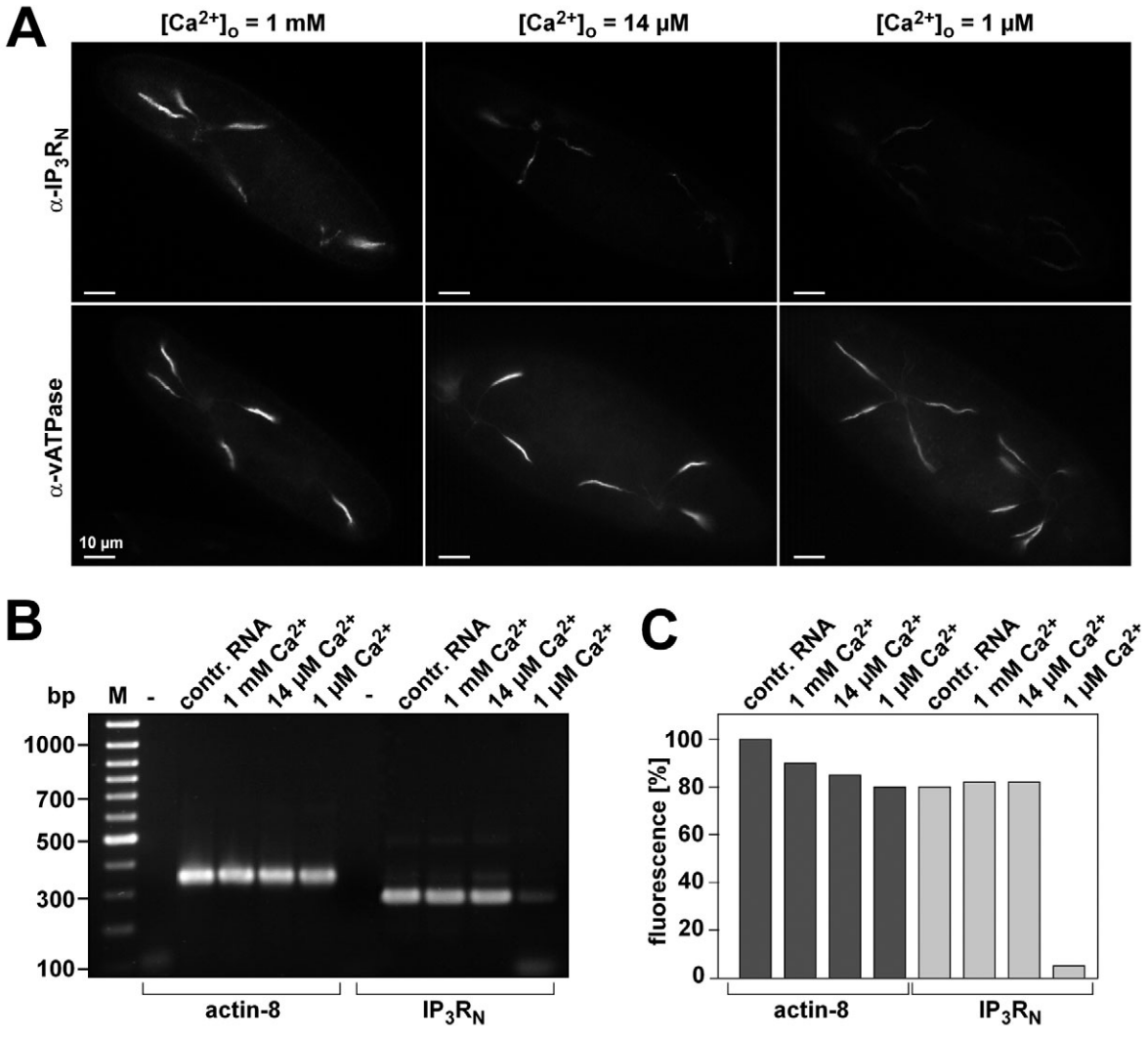

Fig. 6. Influence of extracellular $[Ca^{2+}]_o$ on IP_3R_N gene expression. (A) Immuno-fluorescence images using IP_3R_N-specific Abs (upper panels, α-IP_3R_N) or Abs against V-type H^+-ATPase (lower panels, α-vATPase). Cells were exposed for 24 hours to different levels of $[Ca^{2+}]_o$ as indicated. IP_3R_N seems to be downregulated with decreasing $[Ca^{2+}]_o$. Images were acquired and processed under strictly identical conditions. (B) RNA prepared from cells, which were incubated for 24 hours with different $[Ca^{2+}]_o$, was analyzed by RT-PCR using primers against *Pt*IP_3R_N or against *Pt*actin8 (control). (C) Quantification of fluorescence confirms downregulation of IP_3R_N mRNA compared with actin-8.

the anterior and posterior pole (Fig. 10), when analyzed over larger cell areas. More scrutinized analysis of sites closer to and further away from the ORS showed maximal effects at sites close to the ORS (Fig. 9). In Fig. 9, fluorescence signals were also evaluated from an area of the anterior and posterior part of the cell outside the reach of the corresponding contractile vacuole (Fig. 9, blue and green areas). These signals did not show such a distinctive Ca^{2+} peak as the one close the ORS, and seem to be similar to the spontaneous Ca^{2+} oscillations observed in baseline recordings. Some experiments suggest that the frequency of these signals is influenced by uncaging Ins(1,4,5)P_3 (Fig. 10). Thus, significant changes in the amplitude were seen only in regions where the spongiome is attached to a collecting canal (Fig. 9, red area). The effect of uncaging Ins(1,4,5)P_3 varied from cell to cell as to be expected for a stochastic fine-tuning activity, involving a compartment moderately enriched with Ca^{2+} (see Discussion).

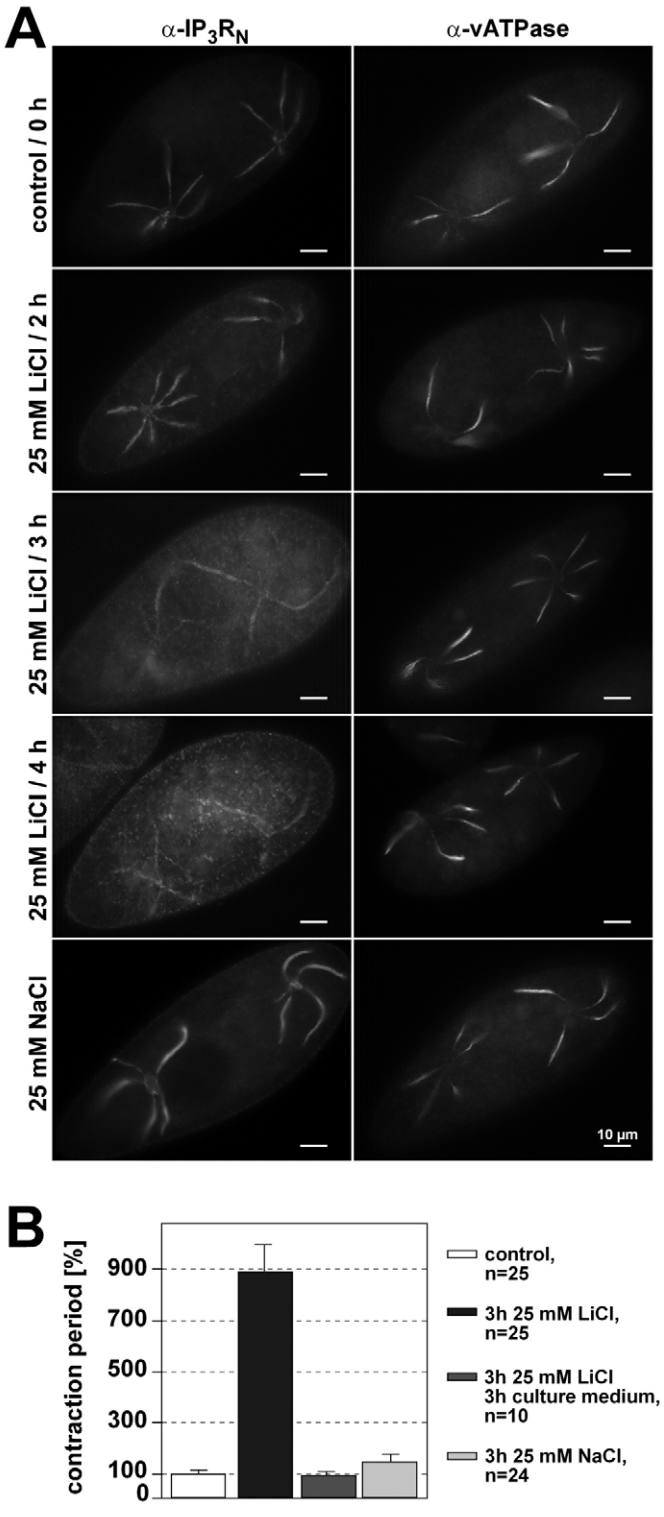

Discussion

We have identified, for the first time on a molecular level an Ins(1,4,5)P_3R in its full length in a protozoan. Since the immunolocalization of IP_3R_N to the ORS was unexpected, we compared its structure in some detail with Ins(1,4,5)P_3Rs of other cells and provide information of its potential role in establishing $[Ca^{2+}]_i$ homeostasis.

Molecular properties of IP_3R_N compared with Ins(1,4,5)P_3Rs from other cells

Investigations of intracellular Ca^{2+} signaling in other protozoa imply the presence of Ins(1,4,5)P_3Rs and RyRs in these organisms. For example, in *Dictyostelium* disruption of the *iplA* gene, encoding an Ins(1,4,5)P_3-receptor-like protein, abolishes Ca^{2+} entry stimulated by ATP or folic acid (Traynor et al., 2000). The relationship of the IplA protein to Ins(1,4,5)P_3Rs is based on homologous regions corresponding to the channel domain and two regions of approximately 200 amino acid residues flanking the Ins(1,4,5)P_3-binding domain. Despite the evidence that Ins(1,4,5)P_3 can cause the release of Ca^{2+} from internal stores in *Dictyostelium* (Flaadt et al., 1993), biochemical evidence that IplA is an Ins(1,4,5)P_3 receptor is still lacking. Furthermore, homologous sequences are also present in the genomes of parasitic protozoa, but so far they have not been cloned. Based on functional analysis in *Toxoplasma gondii*, a parasite and close relative of *Paramecium*, a mixed-type Ca^{2+}-release channel has been postulated (Lovett et al., 2002). In *Paramecium*, one might think of such a mixed type, but despite the described similarity of the IP_3R_N to RyR in its channel region, the overall molecular characteristics are clearly in favor of an Ins(1,4,5)P_3R.

Fig. 7. Li^+ affects subcellular distribution of IP_3R_N. (A) Immunofluorescence analysis of cells grown in media with 1 μM $[Ca^{2+}]_o$ and incubated with 25 mM LiCl for the times indicated, followed by immuno-labeling with IP_3R_N-specific Abs (left panels, α-IP_3R_N) or Abs against V-type H^+-ATPase (right panels, α-vATPase). The IP_3R_N is selectively affected, with a maximal outcome after 3 hours, resulting in reduced ORS-staining and increased diffuse background fluorescence. As a control, cells were treated with NaCl for 3 hours (bottom panels) with no remarkable effect. (B) Contraction periods of contractile vacuoles of cells treated with LiCl for 3 hours are significantly prolonged (black bar) when compared to control cells (white bar, $P<0.001$) or to cells treated with NaCl (light gray bar, $P<0.001$). Contraction periods of cells incubated with NaCl are only slightly prolonged in comparison to control cells, with weak significance ($P=0.014$ for NaCl to untreated control). Three hours after treatment with LiCl, contraction periods return to control levels when cells are transferred to culture medium (dark gray bar).

Appraisal of different effects on IP_3R_N expression

We observed the downregulation of IP_3R_N in the ORS when $[Ca^{2+}]_o$ was greatly reduced. This might imply that, in the absence of significant Ca^{2+} influx into the cell, no Ca^{2+} is sequestered into the ORS and, therefore, no Ca^{2+} is recycled into the cytosol. Experiments with LiCl yielded similar results. From yeast (Navarro-Avino et al., 2003) to mammals (Berridge et al., 1989; Parthasarathy and Parthasarathy, 2004), Li^+ is known to inhibit, though not exclusively, biosynthesis of Ins(1,4,5)P_3 precursors. These data lend further support to a role of Ins(1,4,5)P_3Rs in Ins(1,4,5)P_3-mediated $[Ca^{2+}]_i$ homeostasis. Along those lines, in *Paramecium*, positive chemotactic responses (Wright et al., 1992) that are normally accompanied by Ca^{2+} signals as well as surface pattern formation (Beisson and Ruiz, 1992) are inhibited by LiCl. It is not surprising that, under such conditions of latent activity, no Ins(1,4,5)P_3 formation has been reported in *Paramecium* up to now.

Possible implications for $[Ca^{2+}]_i$ homeostasis

Implications for $[Ca^{2+}]_i$ homeostasis were analyzed by manipulating $[Ca^{2+}]_o$ and $[Ca^{2+}]_i$, based on the fact that $[Ca^{2+}]_i$ in *Paramecium* is rapidly adjusted to levels of Ca^{2+} available in the medium (Browning and Nelson, 1976; Kerboeuf and Cohen, 1990; Erxleben et al., 1997). The general assumption was that the ORS in *Paramecium* not only serves the adjustment of internal hydrostatic pressure but, necessarily, also of the internal ionic milieu. This interplay might be complicated because the H^+-ATPase located in the decorated spongiome (Allen et al., 1990; Fok et al., 1995; Naitoh et al.,

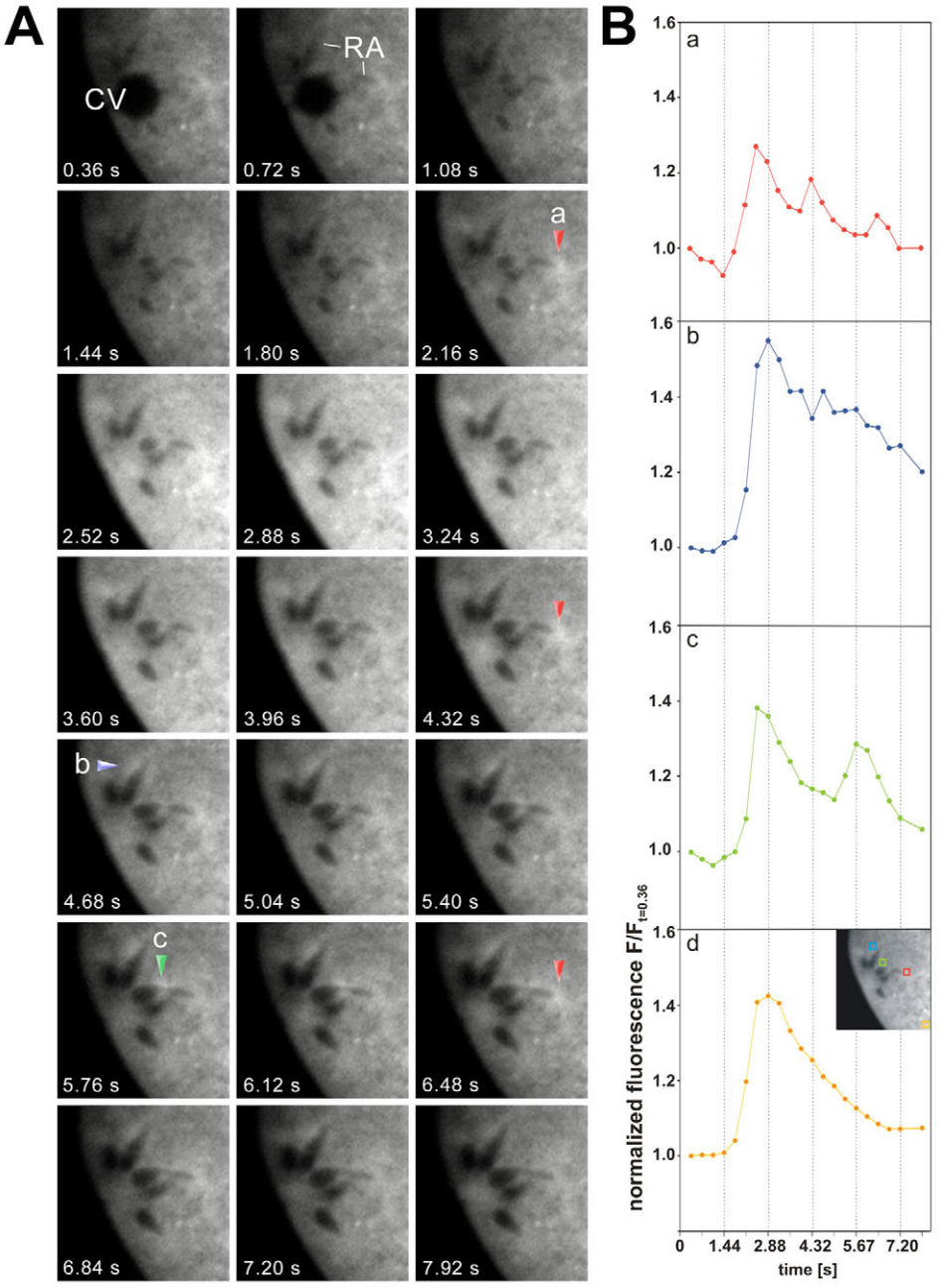

Fig. 8. Recordings of Ca^{2+} signals in close proximity to the ORS. (A) Elevated by a large Ca^{2+} signal traveling through the whole cell, small Ca^{2+} sparks localized close to the ampullae and radial arms (RA) can be observed (arrows) These spontaneous subcellular Ca^{2+} signals move along the ORS (CV, contractile vacuole). (B) Line tracings of the different spots marked by colored arrows in A. Trace d represents the large Ca^{2+} signal which elevates the small additional Ca^{2+} sparks visualized in traces a-c.

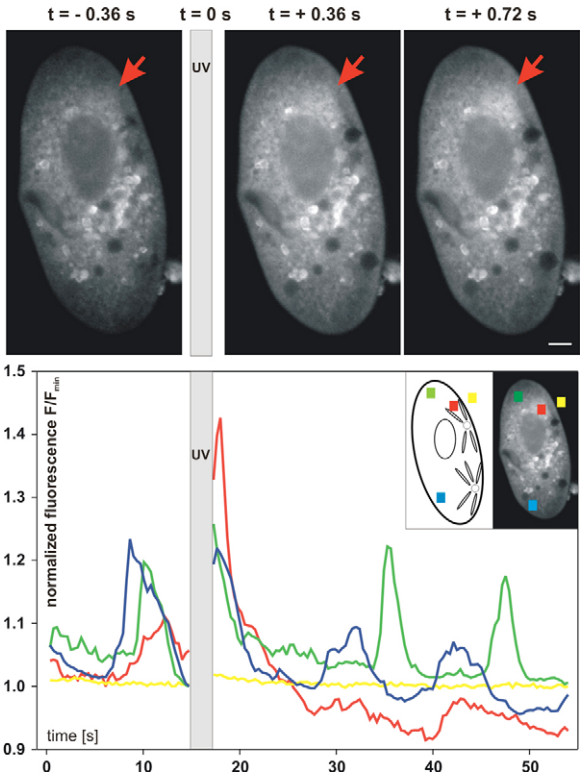

Fig. 9. Effect of Ins(1,4,5)P_3-uncaging on local Ca^{2+} signaling at different distances from the ORS. Recordings of Ca^{2+} signals before (–0.36 seconds) and directly after the release of caged Ins(1,4,5)P_3 by UV light (+0.36 seconds, +0.72 seconds) show an increase in fluorescence after the activation of Ins(1,4,5)P_3 in close proximity to the ORS (arrow) (bar, 10 μm). Graph shows Ca^{2+} traces analyzed from different areas in the cell, which were adjusted to the minimal fluorescence value before UV illumination (F_{min}). During baseline recordings, spontaneous Ca^{2+} signals are observed. Illumination with UV light for 1 second (gray bar), i.e. uncaging of Ins(1,4,5)P_3, results in an increase of the Ca^{2+} signal from the area close to the upper vacuole (red) which is not seen to such an extent in the anterior (green) or posterior (blue) part of the cell.

1997; Tominaga et al., 1998) produces electrogenic force not only for organellar water uptake (Grønlien et al., 2002; Stock et al., 2002a; Stock et al., 2002b), but might also be coupled to a secondary active ion transport by exchangers. Among them, one may envisage a H^+-Ca^{2+}-based or a similar Ca^{2+}-based exchanger, as occurring in acidocalcisomes of some parasitic protozoa (Docampo and Moreno, 2001) and in plant cell vacuoles (Hetherington and Brownlee, 2004). What might be the relative contribution of such a mechanism to overall Ca^{2+} homeostasis?

Assuming, that a *Paramecium* cell has two contractile vacuoles, each releasing a volume of ~100 femtoliters $second^{-1}$ (Grønlien et al., 2002), i.e. 6 picoliters $minute^{-1}$, a total cell volume of 0.7×10^{-10} l (Erxleben et al., 1997), the ORS would discharge 8.6% of the cell volume per minute. Release of a total equivalent of the cell volume would, thus, require 11.6 minutes. Under standard conditions of $[Ca^{2+}]_o$= 1 mM, a $[Ca^{2+}]_{ORS}$= 2.5 mM was found by impaling Ca^{2+}-selective microelectrodes (Stock et al., 2002a; Stock et al., 2002b). Then, 0.29 mM l^{-1} would be released by the ORS per minute. Latent Ca^{2+} influx under similar conditions, as determined by $^{45}Ca^{2+}$-flux measurements with unstimulated cells, is ~2 pM $second^{-1}$ per 10^3 cells (Kerboeuf and Cohen, 1990). Considering the given cell volume, this amounts to an influx of 1.7 mM l^{-1} $minute^{-1}$, which implies that Ca^{2+} expulsion via the ORS requires only 5.9 minutes to compensate for the latent Ca^{2+} influx, disregarding any other extrusion mechanisms. In comparison, Ca^{2+} expulsion via the pumps is known to operate rather sluggishly (Plattner and Klauke, 2001). This makes the ORS an interesting key-player in the regulation not only of cell volume and hydration, but unexpectedly also in $[Ca^{2+}]_i$ homeostasis.

We therefore expected some effect of $[Ca^{2+}]_o$ on the function of the Ins(1,4,5)P_3R. We altered the $[Ca^{2+}]_o$ levels down to 1 μM – a level just above the minimum levels tolerated by *Paramecium* cells over some time (Kerboeuf and Cohen, 1990) and observed that lowering $[Ca^{2+}]_o$ to threshold values greatly reduces the expression of IP_3R_N.

In aggregate, all these findings strongly support our hypothesis that, in *Paramecium*, Ins(1,4,5)P_3Rs serve $[Ca^{2+}]_i$

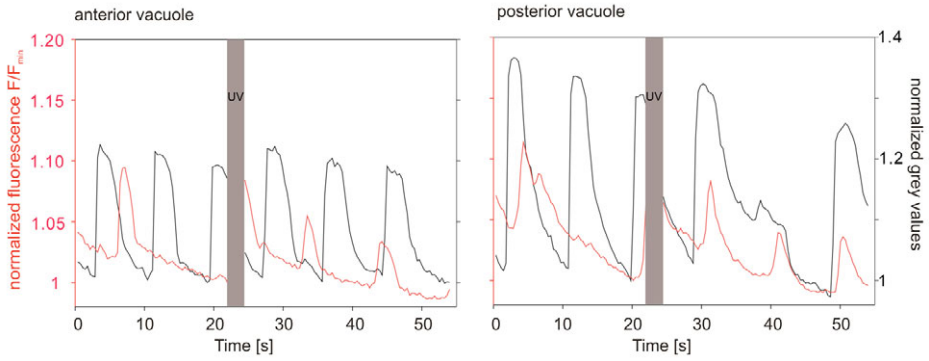

Fig. 10. Effects of Ins(1,4,5)P_3-uncaging on Ca^{2+} oscillations over large areas; anterior (left) and posterior cell poles (right). Recordings of Ca^{2+} signals (red) before and after the release of caged Ins(1,4,5)P_3 by UV light compared to the contraction period (black) of the contractile vacuole. Ca^{2+} signals were recorded on the anterior or posterior part of the same cell, away from contraction sites. Peaks of black curves correspond to the contracted state of the vacuole. During baseline recordings spontaneous Ca^{2+} oscillations are observed. Illumination with UV light (gray bar) for uncaging of Ins(1,4,5)P_3 does not allow to recognize a global increase of Ca^{2+} signals, but affects the periodicity of the oscillating Ca^{2+}-signal.

homeostasis. As in how this might work, one has to consider several aspects. (1) Substantial Ca^{2+} secretion is executed by the ORS, as determined by ion-selective electrodes (Stock et al., 2002a; Stock et al., 2002b). (2) The $[Ca^{2+}]_i$ level actually available depends on the Ca^{2+} influx. (3) This rapidly adjusts to levels of $[Ca^{2+}]_o$ (Browning and Nelson, 1976; Kerboeuf and Cohen, 1990; Erxleben et al., 1997). Based on these arguments it is, therefore, plausible to postulate a counter-acting efflux mechanism operating at the ORS for fine-tuning of $[Ca^{2+}]_i$. Remarkably, this is what happens, on an organismic level, in the kidney nephrons.

Implication of Ca^{2+} signals for the function of IP_3R_N

Our system does not provide the common Ins(1,4,5)P_3-induced Ca^{2+}-response as it is known from mammalian systems, i.e. a large, long-lasting peak. Ca^{2+}-signals induced by uncaging Ins(1,4,5)P_3 seem to be concentrated to the specific region of the cell where the ORS harbors the smooth spongiome with the IP_3R_N we identified in this study. Regarding the [^{3}H]Ins(1,4,5)P_3-binding experiments – which showed a moderate affinity of IP_3R_N for Ins(1,4,5)P_3 – and also the molecular characteristics of IP_3R_N, our receptor mostly resembles the mammalian Ins(1,4,5)P_3R3. These receptors show the lowest affinity for Ins(1,4,5)P_3 but have the strongest affinity for Ca^{2+} of all three types of Ins(1,4,5)P_3R (Miyakawa et al., 1999; Tu et al., 2005). Such a characteristic makes sense if a receptor is involved in latent, fine-tuning processes – such as the tight control of intracellular Ca^{2+}-homoeostasis – and where large volumes of Ca^{2+} releases are not expected. The highly complex feedback-mechanism that regulates activation and inactivation of Ins(1,4,5)P_3Rs involves a suggested cooperative activation of Ins(1,4,5)P_3R by the sequential binding of Ins(1,4,5)P_3 and Ca^{2+} (Adkins and Taylor, 1999; Marchant and Taylor, 1997). Such a coincidence mechanism would explain why uncaging of Ins(1,4,5)P_3 did not result in a consistent change of the spontaneous Ca^{2+} signals already observed by us during baseline recordings. Conditional on the time point when Ins(1,4,5)P_3 was released, the receptors might have been in an inhibited state, depending on the actual Ca^{2+} concentration around the ORS. Their downregulation during exposure to low $[Ca^{2+}]_o$ supports our hypothesis of a role in the regulation of $[Ca^{2+}]_i$ homeostasis.

In sum, the localization of an Ins(1,4,5)P_3 receptor and also the Ins(1,4,5)P_3-dependent Ca^{2+} dynamics coupled to the ORS, underscore the importance of ORS in Ca^{2+} regulation in addition to mere osmoregulation.

Materials and Methods

Paramecium strains and cultivation

P. tetraurelia wild-type stocks *7S* and *d4-2* derived from stock *51S* (Sonneborn, 1974) were cultured as previously described (Kissmehl et al., 2004). For Ca^{2+}-imaging we used the trichocyst non-discharge strain *nd6* (Lefort-Tran et al., 1981).

Genomic-library screening

A genomic library of *P. tetraurelia* macronuclear sequences was screened according to Keller and Cohen (Keller and Cohen, 2000). Specific probes were generated by PCR using IP_3R_N-specific primers p6 5′-aactgcagatatagctattacatttggcttcatc-3′ and p8 5′-aaggaaaaaagcggccgcttctctctttagattttcacttcac-3′.

Sequencing

Sequencing was done by the MWG Biotech (Ebersberg, Germany) custom-sequencing service. DNA sequences were aligned by CLUSTAL W, integrated in DNASTAR Lasergene software package (Madison, WI).

RNA isolation and cDNA preparation

Total RNA was prepared using the RNAgents total RNA Isolation System from Promega (Madison, WI) followed by an additional DNase-I-digestion step. For quantification of RNA transcription levels, cDNA was synthesized using 0.5 μg total RNA (or 5 μg for intron determination) and 0.5 μM of a 3′-anchored dT-primer (5′-aactggaa**gaattc**gcggccgcggaatttttttttttttt-3′; bold characters, *Eco*RI restriction site, underlined characters, *Not*I restriction site).

Intron determination

To identify the complete ORF of IP_3R_N, mRNA sequences were amplified by reverse transcriptase (RT)-PCR. PCR reactions were performed with the Advantage 2 PCR Enzyme System (Clontech, Palo Alto, CA) according to manufacturer's manual, by using 2 μl of cDNA (see above) as template. PCR reactions were carried out in 40 cycles.

Detection of the start codon was done with the following primers: 5′-ataaaaataaatggaaataatcaaaat-3′ (P39), 5′-tcgattgtgagtatttctcatttat-3′ (P40), 5′-aatataatccagtgtggaaatgct-3′ (P41). P39 included the start ATG and the 5′-untranslated region and thus did not bind to the cDNA, whereas P40 starting 5 bp downstream of P39 amplified a product with P41 using cDNA as template allowing further intron analysis. The stop codon was determined with the IP_3R_N-specific primer 5′-gattctataagcaatataaactcat-3′ (p7929f) and the primer 5′-aactggaa**gaattc**gcggccgcgg-3′ (bold characters, *Eco*RI restriction site, underlined characters, *Not*I restriction site) corresponding to the polyA tail of the amplified cDNA (see above). mRNA analysis of the whole receptor was completed using the following primer pairs: 5′-attgtggataattgaggatgaaga-3′ (a-f), 5′-ccatgtctctaattcctgttttgt-3′ (a-rev); 5′-ttgatgtcttattgcagattctg-3′ (b-f), 5′-tacttaacctacaccaaaatgacc-3′ (b-rev); 5′-atttggaatcccagttaagttgag-3′ (c-f), 5′-cttctggttcatcaatctcatcg-3′ (c-rev), 5′-gacgattaaactattaaggctgc-3′ (d-f), 5′-agtgtttaaaagtcttggattgtc-3′ (d-rev); 5′-aaattttcaaagacaatccaagac-3′ (e-f), 5′-tgaatagaaagttgaacaaagtgc-3′ (e-rev); 5′-taattgaattttctagccagtttg-3′ (f-f), 5′-aaaccaattcatttagtgtacca-3′ (f-rev); 5′-cagtaatttaatgtgttgtttgg-3′ (g-f), 5′-aagaaaatatattcattcaaagcc-3′ (g-rev). Amplified cDNA fragments were directly cloned in the pCRII-TOPO cloning system (Invitrogen, Carlsbad, CA) according to the manufacturer's protocol. Plasmid DNA was extracted from bacteria according to standard protocols and were analyzed by sequencing.

Quantification of RNA transcription level

Reverse transcription of 0.5 μg total RNA was performed using Transcriptor reverse transcriptase (Roche, Mannheim, Germany). One-tenth of cDNA samples were amplified by PCR (35 cycles) with the Advantage 2 PCR Enzyme System (Clontech) using *Pt*actin8-specific primers (act8-f: 5′-gctctagatttccagtggaaaaacaaacag-3′; act8-rev: 5′-ccgctcgagaccatcgggcaaatcataca-3′) as control or IP_3R_N-specific primers (ef (see above) and e2rev: 5′-atcgaagatccttttgctaactac-3′).

Computational analysis

BLAST searches were performed at the NCBI database (Altschul et al., 1997). Protein alignments were performed with CLUSTAL W (Thompson et al., 1994). Phylogenetic and molecular evolutionary analyses were performed using MEGA version 3.0 (Kumar et al., 2004). Modeling of protein structures was done using the SWISS-MODEL server (http://swissmodel.expasy.org) for automated comparative modeling (Peitsch et al., 1993). For the IP_3R_N Ins(1,4,5)P_3-binding domain the 'alignment mode' was chosen and the structurally known Ins(1,4,5)P_3-binding domain from mouse Ins(1,4,5)P_3 receptor type 1 (Bosanac et al., 2002) was downloaded from the ExPDB template library. Modeling tasks were handled in 'project mode' using DeepView (Swiss-PdbViewer).

Expression and immuno-precipitation of GFP-fusion protein

Sequences encoding the Ins(1,4,5)P_3-binding domain of IP_3R_N (S268-L658) were amplified by PCR using primers pBD-f (5′-gcgctgcagatgtcaacatcttggaaaattaatctt-3′) and pBD-rev (5′-cgcctcgagaacctaatcgttcaaatagatacaatta-3′), and cloned in a modified pPXV-GFP vector (Wassmer et al., 2005). *Paramecium* cells were transformed by microinjecting DNA into the macronucleus as described by Wassmer et al. (Wassmer et al., 2005). Injected cells were examined for GFP-expression, isolated and grown in excess of bacterized medium to avoid induction of autogamy. Cultures were harvested, washed twice in PIPES-buffer (5 mM Pipes-HCl pH 7, 1 mM KCl, 1 mM $CaCl_2$), frozen in liquid nitrogen and stored at –80°C. GFP and the GFP-fusion protein GFP-IP_3BD were immuno-precipitated with 5 μg/ml of whole-cell homogenate in NET buffer (50 mM Tris-HCl pH 7.4, 5 mM EDTA, 150 mM NaCl, 1% Triton X-100) supplemented with protease inhibitors [15 μM pepstatin A and 42 μM Pefabloc (Serva, Heidelberg, Germany), 100 μM leupeptin and 28 μM E64 (Biomol, Hamburg, Germany), 75 mU ml^{-1} aprotinin, 10 μM chymostatin and 10 μM antipain (Sigma, Munich, Germany)]. 10 μg of affinity-purified anti-GFP Ab (see Wassmer et al., 2006) were added, followed by an 1-hour incubation at 4°C. Immuno-complexes were collected by adding 50 μl of 50% protein A-agarose (Roche) and further incubated for 2 hours. Agarose beads coupled to protein A were washed four times with NET and then divided for [^{3}H]Ins(1,4,5)P_3 binding (see below) and for western blotting experiments. In the latter case, proteins were eluted with 2% SDS for 10 minutes at 37°C.

[^{3}H]Ins(1,4,5)P_3-binding assay

Agarose beads coupled to protein A were washed twice in binding buffer (50 mM Tris-HCl pH 7, 1 mM EDTA), diluted to 100 μl with the binding buffer and incubated with 9.6 nM [^{3}H]Ins(1,4,5)P_3 (Hartmann Analytic GmbH, Braunschweig, Germany) for 40 minutes at 4°C according to Yoshikawa et al. (Yoshikawa et al., 1996). Beads were washed once in binding buffer and dried with a micropipette. [^{3}H]Ins(1,4,5)P_3-protein complexes were eluted with 2% SDS, transferred to 10 ml scintillation fluid (Ready Value Cocktail, Beckman Coulter Inc., Fullerton, CA) and radioactivity was measured in a Beckman liquid scintillation counter. Nonspecific binding was measured in the presence of 10 μM Ins(1,4,5)P_3.

Cloning, expression and purification of an immunogenic peptide

Sequences encoding residues R896-Q1001 of IP_3R_N (IP_3R_N-AG), were cloned into the *Xho*I-*Bam*HI restriction sites of the expression plasmid pET16b (Novagen, Madison, WI). All deviating *Paramecium* glutamine codons (TAA, TAG) were changed to the universal code by PCR methods (Dillon and Rosen, 1993). His_{10}-tagged fusion protein His-IP_3R_N-AG was overexpressed in the *E.coli* strain BL21(DE3) and purified in a two-step procedure. After 3 hours of induction with 1 mM isopropyl-β-D-thiogalactopyranoside (IPTG), bacteria were pelleted and resuspended in ddH_2O containing 20 μg/ml lysozyme and were stored overnight at –20°C. After thawing, Triton X-100 was added to a final concentration of 0.5%. Lysed bacteria were sonicated (1 minute; 80 W) and centrifuged at 30,000 ***g*** for 20 minutes (4°C). The supernatant was removed and the pellet (pre-purified inclusion bodies) was resuspended in 6 M guanidine hydrochloride (complemented with 0.1 M Na_2HPO_4) in 0.01 M Tris-HCl buffer pH 8. Further purification steps were performed by using immobilized metal-ion-affinity-chromatography under denaturing conditions according to manufacturer's protocol (Novagen).

Generation and affinity purification of Abs

Polyclonal Abs were raised in rabbits by repeated injection of purified His-IP_3R_N-AG fusion protein. The obtained serum was purified in a two-step procedure. First, anti-His-tag Abs were removed by negative adsorption against an immobilized His-tagged protein. The flow-through was collected and applied to a column containing immobilized His-IP_3R_N-AG fusion protein. After adsorption of His-IP_3R_N-AG-specific Abs, the column was washed with 20 column volumes of NET (150 mM NaCl, 50 mM Tris-HCl pH 8, 5 mM EDTA, 0.5% NP-40), 20 column volumes of NET containing 1 M NaCl, 10 column volumes of NET without NP40 and 5 column volumes TE (10 mM Tris-HCl pH 8, 1 mM EDTA). Bound Abs were eluted with 0.5 column volumes of 100 mM Na citrate (pH 2.5) and immediately neutralized with 1 M Tris-HCl pH 8.

Cell fractionation and western blot analysis

Paramecium cells (stock *7S*) were grown in sterile media, harvested and washed twice in PIPES-buffer. Whole cell homogenates were prepared by lysing cells in 20 mM tri-ethanolamine (TEA) pH 7.4, 15% glycerol (4°C). Insoluble material was pelleted by centrifugation at 100,000 ***g*** for 45 minutes. The supernatant was removed and the pellet was resuspended in 20 mM TEA pH 7.4, 7.5% glycerol. After protein determination, Triton X-100, NaCl, EDTA and Tris-HCl pH 7.5 was added to a final concentration of 1.5%, 150 mM, 5 mM and 50 mM. Membrane-bound proteins were eluted on ice for 20 minutes, followed by an additional centrifugation step (30 minutes, 40,000 ***g***, 4°C). Proteins (50 μg of each fraction) were separated on 5-10% SDS polyacrylamide gel electrophoresis (PAGE), transferred onto nitrocellulose membranes, and treated with specific Abs. Protease inhibitors were added to all buffers used from cell disruption on as described above.

Immuno-labeling of *Paramecium* cells and fluorescence microscopy

Paramecium cells (stock *7S*) suspended in PIPES-buffer or in culture media were fixed in 4% formaldehyde (in phosphate-buffered saline, PBS) and digitonin (Sigma) was added immediately to a final concentration of 0.5%. After 30 minutes of incubation, cells were washed in PBS, followed by two incubations in PBS; 50 mM glycine and finally in PBS complemented with bovine serum albumin (BSA, 1%). Cells were then exposed for 1 hour to the primary antibody in PBS with 1% BSA. Affinity-purified anti-IP_3R_N Abs were used at a concentration of 6 μg/ml. Primary Abs against V-type H^+-ATPase were previously described by Wassmer et al. (Wassmer et al., 2006) [there designated as anti a1-1 (P178–S328)] and used at a concentration of 12 μg ml^{-1}. Afterwards, cells were washed 3 times in PBS followed by the incubation (1 hour) with Alexa Fluor-488-conjugated anti-rabbit Abs (Molecular Probes, Eugene, OR) diluted 1:150 in PBS with 1% BSA. After six rinses in PBS, cells were analyzed in an epifluorescence Axiovert 100TV microscope (Carl Zeiss, Jena, Germany) equipped with FITC-filterset 9 and with a ProgRes C10 plus camera (Jenoptik, Jena, Germany). Images were captured using ProCa 2.0 software (Carl Zeiss) and further processed with Adobe Photoshop (Adobe Systems, San Jose, CA) under identical conditions.

Electron microscopy

The method applied was as indicated by Kissmehl et al. (Kissmehl et al., 2004). Briefly, cells were injected into 8% formaldehyde + 0.1% glutaraldehyde, pH 7.2, 0°C, using a quenched-flow machine and processed by the 'progressive lowering of the temperature'-method. This involved stepwise reduction of the temperature, with increasing ethanol concentrations, followed by LR Gold methacrylate resin-embedding and UV polymerization at –35°C. Anti-IP_3R_N Abs have been used for immuno-gold localization by protein-A-gold conjugated to 5-nm gold (Au_5) in a Zeiss electron microscope, EM10.

Functional analysis with varying $[Ca^{2+}]_o$ and with Li^+

Paramecium cells (stock *d4-2*) were centrifuged (2 minutes, 180 ***g***) and suspended in the experimental solution, with two changes. Different $[Ca^{2+}]_o$ concentrations were adjusted by adding 2 mM, 1 mM or 0.85 mM $CaCl_2$ to 5 mM Pipes pH 7, 1 mM KCl, 1 mM EGTA. Free $[Ca^{2+}]_o$ was calculated according to Patton et al. (Patton et al., 2004) using the MaxChelator program Winmaxc v.2.40. Experiments with LiCl have been carried out as described by Beisson and Ruiz (Beisson and Ruiz, 1992). A 2 M LiCl stock solution was diluted to 25 mM in an exponentially growing culture, where the number of cells was adjusted to 10^3 cells per ml culture media supplemented with 1 mM EGTA and 0.85 mM Ca^{2+} to get a final concentration of 1 μM $[Ca^{2+}]_o$. Cells were incubated with LiCl for the times indicated and then analyzed by immuno-labeling (see above). The contraction periods of contractile vacuoles were measured in cells contained in a microdrop overlaid with paraffin oil.

$[Ca^{2+}]_i$ fluorochrome measurements

P. tetraurelia (strain *nd6*) cells were isolated in microdrops of PIPES-buffer with 0.2% BSA added and covered with paraffin oil. After cautious reduction of the droplet volume to immobilize the cells, they were injected using the Eppendorf injection system consisting of the Injectman NI2, Femtojet and Femtotips I (Eppendorf, Hamburg, Germany). As a Ca^{2+}-fluochrome we used the high-affinity dextran-coupled Fluo-4 (10,000 kDa, Molecular Probes). The volume injected was ~5-10% of the cell volume. For injection 17 mg/ml dextran-coupled Fluo-4 was used either alone or together with 670 μM NPE-caged Ins(1,4,5)P_3 (Molecular Probes) both dissolved in 10 mM Tris-HCl pH 7.2. After injection, cells were flooded for a recovery period of 15-30 minutes. Then cells were immobilized again and Fluo-4 signals were recorded with a 40× α-plan Neofluar objective, NA 0.75, on an Axiovert 200 M microscope equipped with an Axiocam MRm digital camera (Carl Zeiss). Excitation light (50-65% intensity) was selected from a 100 W HBO lamp.

Fluorescent Ca^{2+}-signals were recorded using the Axiovision 4.3 Software (Carl Zeiss). For uncaging of Ins(1,4,5)P_3 cells were locally illuminated for ~1 second with UV light which was selected by filterset 49 with excitation at 365 nm and emission at 445 nm. Recordings were done in a 2×2 binning mode, with an illumination time of 150 milliseconds, pictures were taken every 360 milliseconds.

We gratefully acknowledge the help of Jochen Hentschel with some data processing steps and the excellent technical assistance of Ruth Hohenberger and Lauretta Nejedli. We thank especially Jean Cohen and Linda Sperling (CNRS, Gif-sur-Yvette, France) for enabling us to perform the screening experiments and for providing access to the developing *Paramecium* genome project at an early stage. Additionally we thank Claudia Stuermer for the use of the microscope for Ca^{2+} imaging. Work was supported by the Deutsche Forschungsgemeinschaft, grant to H.P., project TR-SFB11/C4.

References

Adkins, C. E. and Taylor, C. W. (1999). Lateral inhibition of inositol 1,4,5-trisphosphate receptors by cytosolic Ca(2+). *Curr. Biol.* **9**, 1115-1118.

Allen, R. D. (1995). Membrane tubulation and proton pumps. *Protoplasma* **189**, 1-8.

Allen, R. D. and Naitoh, Y. (2002). Osmoregulation and contractile vacuoles of protozoa. *Int. Rev. Cytol.* **215**, 351-394.

Allen, R. D., Ueno, M. S., Pollard, L. W. and Fok, A. K. (1990). Monoclonal antibody study of the decorated spongiome of contractile vacuole complexes of *Paramecium*. *J. Cell Sci.* **96**, 469-475.

Altschul, S. F., Madden, T. L., Schäffer, A. A., Zhang, J., Zhang, Z., Miller, W. and Lipman, D. J. (1997). Gapped BLAST and PSI-BLAST: a new generation of protein database search programs. *Nucleic Acids Res.* **25**, 3389-3402.

Beisson, J. and Ruiz, F. (1992). Lithium-induced respecification of pattern in *Paramecium*. *Dev. Genet.* **13**, 194-202.

Berridge, M. J., Downes, C. P. and Hanley, M. R. (1989). Neural and developmental actions of lithium: a unifying hypothesis. *Cell* **59**, 411-419.

Berridge, M. J., Lipp, P. and Bootman, M. D. (2000). The versatility and universality of calcium signalling. *Nat. Rev. Mol. Cell Biol.* **1**, 11-21.

Bezprozvanny, I. (2005). The inositol 1,4,5-trisphosphate receptors. *Cell Calcium* **38**, 261-272.

Blondel, O., Takeda, J., Janssen, H., Seino, S. and Bell, G. I. (1993). Sequence and

functional characterization of a third inositol trisphosphate receptor subtype, IP_3R-3, expressed in pancreatic islets, kidney, gastrointestinal tract, and other tissues. *J. Biol. Chem.* **268**, 11356-11363.

Bosanac, I., Alattia, J. R., Mal, T. K., Chan, J., Talarico, S., Tong, F. K., Tong, K. I., Yoshikawa, F., Furuichi, T., Iwai, M. et al. (2002). Structure of the inositol 1,4,5-trisphosphate receptor binding core in complex with its ligand. *Nature* **420**, 696-700.

Browning, J. L. and Nelson, D. L. (1976). Biochemical studies of the excitable membrane of *Paramecium aurelia*. I. $^{45}Ca^{2+}$ fluxes across resting and excited membrane. *Biochim. Biophys. Acta* **448**, 338-351.

Dessen, P., Zagulski, M., Gromadka, R., Plattner, H., Kissmehl, R., Meyer, E., Bétermier, M., Schultz, J. E., Linder, J. U., Pearlman, R. E. et al. (2001). *Paramecium* genome survey: a pilot project. *Trends Genet.* **17**, 306-308.

Dillon, P. J. and Rosen, C. A. (1993). Use of polymerase chain reaction for the rapid construction of synthetic genes. *Methods Mol. Biol.* **15**, 263-269.

Docampo, R. and Moreno, S. N. J. (2001). The acidocalcisome. *Mol. Biochem. Parasitol.* **33**, 151-159.

Erxleben, C., Klauke, N., Flötenmeyer, M., Blanchard, M.-P., Braun, C. and Plattner, H. (1997). Microdomain Ca^{2+} activation during exocytosis in *Paramecium* cells. Superposition of local subplasmalemmal calcium store activation by local Ca^{2+} influx. *J. Cell Biol.* **136**, 597-607.

Flaadt, H., Jaworski, E., Schlatterer, C. and Malchow, D. (1993). Cyclic AMP- and Ins(1,4,5)P_3-induced Ca^{2+} fluxes in permeabilised cells of *Dictyostelium discoideum*: cGMP regulates Ca^{2+} entry across the plasma membrane. *J. Cell Sci.* **105**, 255-261.

Fok, A. K., Aihara, M. S., Ishida, M., Nolta, K. V., Steck, T. L. and Allen, R. D. (1995). The pegs on the decorated tubules of the contractile vacuole complex of *Paramecium* are proton pumps. *J. Cell Sci.* **108**, 3163-3170.

Gee, N. S., Ragan, C. I., Watling, K. J., Aspley, S., Jackson, R. G., Reid, G. G., Gani, D. and Shute, J. K. (1988). The purification and properties of myo-inositol monophosphatase from bovine brain. *Biochem. J.* **249**, 883-889.

Grønlien, H. K., Stock, C., Aihara, M. S., Allen, R. D. and Naitoh, Y. (2002). Relationship between the membrane potential of the contractile vacuole complex and its osmoregulatory activity in *Paramecium multimicronucleatum*. *J. Exp. Biol.* **205**, 3261-3270.

Hallcher, L. M. and Sherman, W. R. (1980). The effects of lithium ion and other agents on the activity of myo-inositol-1-phosphatase from bovine brain. *J. Biol. Chem.* **255**, 10896-10901.

Hauser, K., Pavlovic, N., Kissmehl, R. and Plattner, H. (1998). Molecular characterization of a sarco(endo)plasmic reticulum Ca^{2+}-ATPase gene from *Paramecium tetraurelia* and localization of its gene product to sub-plasmalemmal calcium stores. *Biochem. J.* **334**, 31-38.

Hetherington, A. M. and Brownlee, C. (2004). The generation of Ca^{2+} signals in plants. *Annu. Rev. Plant Biol.* **55**, 401-427.

Keller, A. M. and Cohen, J. (2000). An indexed genomic library for *Paramecium* complementation cloning. *J. Eukaryot. Microbiol.* **47**, 1-6.

Kerboeuf, D. and Cohen, J. (1990). A Ca^{2+} influx associated with exocytosis is specifically abolished in a *Paramecium* exocytotic mutant. *J. Cell Biol.* **111**, 2527-2535.

Kissmehl, R., Huber, S., Kottwitz, B., Hauser, K. and Plattner, H. (1998). Subplasmalemmal Ca-stores in *Paramecium tetraurelia*. Identification and characterization of a sarco(endo)plasmic reticulum-like Ca^{2+}-ATPase by phosphoenzyme intermediate formation and its inhibition by caffeine. *Cell Calcium* **24**, 193-203.

Kissmehl, R., Sehring, I. M., Wagner, E. and Plattner, H. (2004). Immuno-localization of actin in *Paramecium* cells. *J. Histochem. Cytochem.* **52**, 1543-1559.

Knoll, G., Kerboeuf, D. and Plattner, H. (1992). A rapid calcium influx during exocytosis in *Paramecium* cells is followed by a rise in cyclic GMP within 1s. *FEBS Lett.* **304**, 265-268.

Knoll, G., Grassle, A., Braun, C., Probst, W., Hohne-Zell, B. and Plattner, H. (1993). A calcium influx is neither strictly associated with nor necessary for exocytotic membrane fusion in *Paramecium* cells. *Cell Calcium* **14**, 173-183.

Kumar, S., Tamura, K. and Nei, M. (2004). MEGA3: integrated software for molecular evolutionary genetics analysis and sequence alignment. *Brief. Bioinform.* **5**, 150-163.

Laenge, S., Klauke, N. and Plattner, H. (1995). Subplasmalemmal Ca^{2+} stores of probable relevance for exocytosis in *Paramecium*. Alveolar sacs share some but not all characteristics with sarcoplasmic reticulum. *Cell Calcium* **17**, 335-344.

Lefort-Tran, M., Aufderheide, K., Phouphile, M., Rossignol, M. and Beisson, J. (1981). Control of exocytotic processes: cytological and physiological studies of trichocyst mutants in *Paramecium tetraurelia*. *J. Cell Biol.* **88**, 301-311.

Lovett, J. L., Marchesini, N., Moreno, S. N. J. and Sibley, L. D. (2002). *Toxoplasma gondii* microneme secretion involves intracellular Ca^{2+} release from inositol 1,4,5-trisphosphate (IP_3)/ryanodine-sensitive stores. *J. Biol. Chem.* **277**, 25870-25876.

Machemer, H. (1988). Electrophysiology. In *Paramecium* (ed. H. D. Görtz), pp. 185-215. Berlin, Heidelberg: Springer-Verlag.

Marchant, J. S. and Taylor, C. W. (1997). Cooperative activation of IP_3 receptors by sequential binding of IP_3 and Ca^{2+} safeguards against spontaneous activity. *Curr. Biol.* **7**, 510-518.

Miyakawa, T., Maeda, A., Yamazawa, T., Hirose, K., Kurosaki, T. and Iino, M. (1999). Encoding of Ca^{2+} signals by differential expression of IP_3 receptor subtypes. *EMBO J.* **18**, 1303-1308.

Naitoh, Y., Tominaga, T., Ishida, M., Fok, A. K., Aihara, M. S. and Allen, R. D. (1997). How does the contractile vacuole of *Paramecium multimicronucleatum* expel fluid? Modeling of the expulsion mechanism. *J. Exp. Biol.* **200**, 713-721.

Navarro-Avino, J. P., Belles, J. M. and Serrano, R. (2003). Yeast inositol mono- and trisphosphate levels are modulated by inositol monophosphatase activity and nutrients. *Biochem. Biophys. Res. Commun.* **302**, 41-45.

Parthasarathy, S. R. S. and Parthasarathy, R. N. (2004). Lithium modulation of the human inositol monophosphatase 2 (IMPA2) promotor. *Biochem. Biophys. Res. Commun.* **324**, 1370-1378.

Patton, C., Thompson, S. and Epel, D. (2004). Some precautions in using chelators to buffer metals in biological solutions. *Cell Calcium* **35**, 427-431.

Peitsch, M. C. and Jongeneel, C. V. (1993). A 3-D model for the CD40 ligand predicts that it is a compact trimer similar to the tumor necrosis factors. *Int. Immunol.* **5**, 233-238.

Plattner, H. and Klauke, N. (2001). Calcium in ciliated protozoa: sources, regulation, and calcium-regulated cell functions. *Int. Rev. Cytol.* **201**, 115-208.

Pointing, C. P. (2000). Novel repeats in ryanodine and IP_3 receptors and protein O-mannosyltransferases. *Trends Biochem. Sci.* **25**, 48-50.

Russell, C. B., Fraga, D. and Hinrichsen, R. D. (1994). Extremely short 20-33 nucleotide introns are the standard length in *Paramecium tetraurelia*. *Nucleic Acids Res.* **22**, 1221-1225.

Serysheva, I. I., Bare, D. J., Ludtke, S. J., Kettlun, C. S., Chiu, W. and Mignery, G. A. (2003). Structure of the type 1 inositol 1,4,5-trisphosphate receptor revealed by electron cryomicroscopy. *J. Biol. Chem.* **278**, 21319-21322.

Sonneborn, T. M. (1974). *Paramecium aurelia.* In *Handbook of Genetics.* Vol. 2 (ed. R. C. Kung), pp. 469-594. New York: Plenum Press.

Sperling, L., Dessen, P., Zagulski, M., Pearlman, R. E., Migdalski, A., Gromadka, R., Froissard, M., Keller, A. M. and Cohen, J. (2002). Random sequencing of *Paramecium* somatic DNA. *Eukaryotic Cell* **1**, 341-352.

Stelly, N., Mauger, J. P., Keryer, G., Claret, M. and Adoutte, A. (1991). Cortical alveoli of *Paramecium*: a vast submembraneous calcium storage compartment. *J. Cell Biol.* **113**, 103-112.

Stock, C., Grønlien, H. K. and Allen, R. D. (2002a). The ionic composition of the contractile vacuole fluid of *Paramecium* mirrors ion transport across the plasma membrane. *Eur. J. Cell Biol.* **81**, 505-515.

Stock, C., Grønlien, H. K., Allen, R. D. and Naitoh, Y. (2002b). Osmoregulation in *Paramecium*: in situ ion gradients permit water to cascade through the cytosol to the contractile vacuole. *J. Cell Sci.* **115**, 2339-2348.

Tatusova, T. A. and Madden, T. L. (1999). Blast 2 sequences – a new tool for comparing protein and nucleotide sequences. *FEMS Microbiol. Lett.* **174**, 247-250.

Thompson, J. D., Higgins, D. G. and Gibson, T. J. (1994). CLUSTAL W: improving the sensitivity of progressive multiple sequence alignment through sequence weighting, position-specific gap penalties and weight matrix choice. *Nucleic Acids Res.* **22**, 4673-4680.

Tominaga, T., Allen, R. D. and Naitoh, Y. (1998). Electrophysiology of the in situ contractile vacuole complex of *Paramecium* reveals its membrane dynamics and electrogenic site during osmoregulatory activity. *J. Exp. Biol.* **201**, 451-460.

Traynor, D., Milne, J. L., Insall, R. H. and Kay, R. R. (2000). Ca^{2+} signalling is not required for chemotaxis in Dictyostelium. *EMBO J.* **19**, 4846-4854.

Tu, H., Wang, Z. and Bezprozvanny, I. (2005). Modulation of mammalian inositol 1,4,5-trisphosphate receptor isoforms by calcium: a role of calcium sensor region. *Biophys. J.* **88**, 1056-1069.

Wassmer, T., Froissard, M., Plattner, H., Kissmehl, R. and Cohen, J. (2005). The vacuolar proton-ATPase plays a major role in several membrane-bounded organelles in *Paramecium*. *J. Cell Sci.* **118**, 2813-2825.

Wassmer, T., Kissmehl, R., Cohen, J. and Plattner, H. (2006). Seventeen a-subunit isoforms of *Paramecium* V-ATPase provide high specialization in localization and function. *Mol. Biol. Cell* **17**, 917-930.

Wright, M. V. and VanHouten, J. L. (1990). Characterization of a putative Ca^{2+}-transporting Ca^{2+}-ATPase in the pellicles of *Paramecium tetraurelia*. *Biochim. Biophys. Acta* **1029**, 241-251.

Wright, M. V., Frantz, M. and Van Houten, J. L. (1992). Lithium fluxes in *Paramecium* and their relationship to chemosresponse. *Biochim. Biophys. Acta* **1107**, 223-230.

Yamauchi, K., Tada, H. and Usuki, I. (1995). Structure and evolution of *Paramecium* hemoglobin genes. *Biochim. Biophys. Acta* **1264**, 53-62.

Yoshikawa, F., Morita, M., Monkawa, T., Michikawa, T., Furuichi, T. and Mikoshiba, K. (1996). Mutational analysis of the ligand binding site of the inositol 1,4,5-trisphosphate receptor. *J. Biol. Chem.* **271**, 18277-18282.

Zagulski, M., Nowak, J. K., Le Mouel, A., Nowacki, M., Migdalski, A., Gromadka, R., Noel, B., Blanc, I., Dessen, P., Wincker, P. et al. (2004). High coding density on the largest *Paramecium tetraurelia* somatic chromosome. *Curr. Biol.* **14**, 1397-1404.